apoE isoform–specific disruption of amyloid β peptide clearance from mouse brain

Rashid Deane,[1] Abhay Sagare,[1] Katie Hamm,[1] Margaret Parisi,[1] Steven Lane,[1] Mary Beth Finn,[2] David M. Holtzman,[2] and Berislav V. Zlokovic[1]

[1]Center for Neurodegenerative and Vascular Brain Disorders and Frank P. Smith Laboratory for Neuroscience and Neurosurgical Research, Department of Neurosurgery, University of Rochester Medical School, Rochester, New York, USA. [2]Department of Neurology, Hope Center for Neurological Disorders, and Alzheimer's Disease Research Center, Washington University School of Medicine, St. Louis, Missouri, USA.

Neurotoxic amyloid β peptide (Aβ) accumulates in the brains of individuals with Alzheimer disease (AD). The *APOE4* allele is a major risk factor for sporadic AD and has been associated with increased brain parenchymal and vascular amyloid burden. How apoE isoforms influence Aβ accumulation in the brain has, however, remained unclear. Here, we have shown that apoE disrupts Aβ clearance across the mouse blood-brain barrier (BBB) in an isoform-specific manner (specifically, apoE4 had a greater disruptive effect than either apoE3 or apoE2). Aβ binding to apoE4 redirected the rapid clearance of free Aβ40/42 from the LDL receptor–related protein 1 (LRP1) to the VLDL receptor (VLDLR), which internalized apoE4 and Aβ-apoE4 complexes at the BBB more slowly than LRP1. In contrast, apoE2 and apoE3 as well as Aβ-apoE2 and Aβ-apoE3 complexes were cleared at the BBB via both VLDLR and LRP1 at a substantially faster rate than Aβ-apoE4 complexes. Astrocyte-secreted lipo-apoE2, lipo-apoE3, and lipo-apoE4 as well as their complexes with Aβ were cleared at the BBB by mechanisms similar to those of their respective lipid-poor isoforms but at 2- to 3-fold slower rates. Thus, apoE isoforms differentially regulate Aβ clearance from the brain, and this might contribute to the effects of *APOE* genotype on the disease process in both individuals with AD and animal models of AD.

Introduction

Dementia in Alzheimer disease (AD) is associated with cerebrovascular dysfunction (1, 2), accumulation of neurotoxic amyloid β peptide (Aβ) in the wall of blood vessels and in the brain parenchyma (3–5), and intraneuronal lesions in the form of neurofibrillary tangles (6–8). Aβ is central to AD pathology (3, 4, 8, 9–12). According to the current concept, Aβ that accumulates in the brain in AD is likely due to its faulty clearance from the brain (10, 11, 13–15). LDL receptor–related protein 1 (LRP1) is a major efflux transporter for Aβ at the blood-brain barrier (BBB) (5, 16, 17). Binding of Aβ to LRP1 at the abluminal side of the BBB in vivo initiates a rapid Aβ clearance from brain to blood via transcytosis across the BBB (16–19). Aβ binding to LRP1 cluster IV expressed at the basolateral side of the kidney epithelial monolayers leads to Aβ internalization and degradation (20).

apoE genotype has a significant effect on the development of AD. apoE4 allele is a major genetic risk factor for sporadic AD, whereas apoE2 allele decreases the risk for AD (reviewed in ref. 21). The exact mechanism by which apoE influences the onset and progression of AD is not completely understood. By acting as an Aβ chaperone molecule, apoE appears to influence brain Aβ metabolism, deposition, toxicity, fibril formation, and clearance (22–25). Murine apoE and human apoE isoforms facilitate in vivo brain Aβ fibrillogenesis in different mouse models of AD, e.g., murine apoE>>apoE4>apoE3 (22, 23, 26–29). apoE4 also promotes the formation of cerebral amyloid angiopathy (CAA) in a mouse model of AD (30). Human apoE3 and apoE4 can both substantially increase parenchymal deposition of fibrillar Aβ in a mouse model of familial Dutch and Iowa CAA (31).

Although several studies have suggested that apoE may retain Aβ in brain parenchyma (11), little is known about the effects of apoE isoforms on clearance of Aβ from brain across the BBB. Here, we report that apoE disrupts Aβ clearance at the BBB in an isoform-specific manner (e.g., apoE4>apoE3 or apoE2) by redirecting a rapid clearance of unbound free Aβ40 and Aβ42 from LRP1 to the VLDL receptor (VLDLR), a receptor with a substantially slower endocytotic rate compared with LRP1 (32), which we show acts to slowly clear apoE and Aβ-apoE complexes.

Results

First, we used our brain tissue clearance technique (16, 17, 19) to compare the disappearance curves from brain interstitial fluid (ISF) of ^{125}I-radiolabeled lipid-poor recombinant human apoE isoforms, astrocyte-derived lipo-apoE isoforms (33), unbound free monomeric synthetic human Aβ40 and Aβ42 peptides, and complexes of various apoEs with Aβ40 and Aβ42. Different apoE and Aβ test tracers and their complexes were microinfused into brain ISF at equimolar concentration of 40 nM simultaneously with ^{14}C-inulin (reference marker). Clearance was measured over a period of 30 to 300 minutes. It is of note that clearance rates of unlabeled and corresponding ^{125}I-labeled apolipoproteins and Aβ have been shown to be almost identical (19). Total efflux from brain ISF of lipid-poor apoE isoforms corrected for degradation (see below) was significantly slower than that of Aβ40 or Aβ42 (Figure 1A).

The analysis of 2 transport components contributing to total efflux of undegraded ligands from brain indicated less efficient efflux across the BBB of apoE isoforms compared with Aβ isoforms, whereas transport by ISF bulk flow was very slow and similar for all test tracers studied (Figure 1B). apoE4 was cleared

Nonstandard abbreviations used: Aβ, amyloid β peptide; APP, Aβ precursor protein; AD, Alzheimer disease; BBB, blood-brain barrier; c.p.m., counts per minute; CSF, cerebrospinal fluid; ISF, interstitial fluid; LDLR, LDL receptor; LRP1, LDLR-related protein 1; VLDLR, VLDL receptor.

Conflict of interest: The authors have declared that no conflict of interest exists.

Citation for this article: *J. Clin. Invest.* **118**:4002–4013 (2008). doi:10.1172/JCI36663.

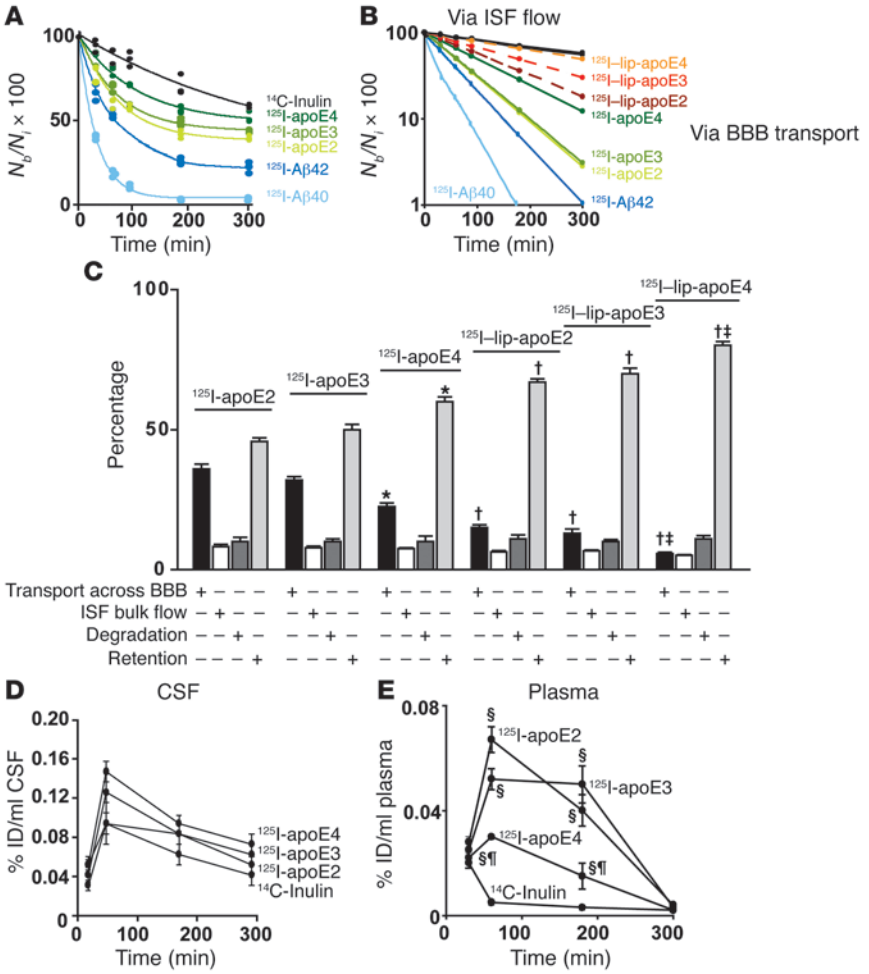

Figure 1

apoE isoform–specific clearance across the mouse BBB in vivo. (**A**) Time-disappearance curves of ^{14}C-inulin (reference molecule, black) and ^{125}I-labeled human lipid-poor apoE4 (dark green), apoE3 (light green), apoE2 (yellow green), Aβ42 (dark blue), and Aβ40 (light blue) after microinfusion of tracers mixture into brain ISF in the caudate nucleus. Test tracers were studied at 40 nM. The percentage recovery in brain was calculated using Equation 1 (see Methods). TCA-precipitable ^{125}I-radioactivity was used. Each point represents a single experiment. (**B**) Time-dependent efflux across the BBB of ^{125}I-labeled Aβ40, Aβ42, lipid-poor apoE2, apoE3, and apoE4 (yellow green, light green, dark green) and lipo-apoE2 (brown), lipo-apoE3 (red), and lipo-apoE4 (orange) was calculated from data in Figure 1A and Equation 4 (see Methods). The ISF bulk flow for studied test tracers was calculated using Equation 2 (see Methods). (**C**) Relative contributions of transport across the BBB (black bars), ISF flow (white bars), and degradation (dark gray bars) to clearance of apoE isoforms from brain and their retention in the brain (light gray bars) were studied at 40 nM concentrations and calculated from fractional coefficients given in Supplemental Table 1. Mean ± SEM; n = 11–24 mice per group for multiple-time series. *$P < 0.05$, lipid-poor apoE4 versus lipid-poor apoE3 or apoE2; †$P < 0.05$, lipo-apoE4, lipo-apoE3, and lipo-apoE2 versus corresponding lipid-poor apoE4, apoE2 and apoE3. ‡$P < 0.05$, lipo-apoE4 versus lipo-apoE3 or lipo-apoE2. (**D** and **E**) Time-appearance curves of ^{14}C-inulin and ^{125}I-labeled lipid-poor apoE4, apoE3, and apoE2 (TCA-precipitable ^{125}I-radioactivity) in the CSF (**D**) and plasma (**E**) from experiments as in **A**. ID, injected dose. §$P < 0.05$, apoE2, apoE3, and apoE4 versus inulin; ¶$P < 0.05$, apoE4 versus apoE2 or apoE3. Mean ± SEM; n = 3–5 mice per group.

at a considerably slower rate across BBB compared with apoE3 or apoE2, as indicated by the respective slopes of the radioactivity disappearance curves at the BBB (Figure 1B). Lipidation favored apoE retention in the brain in an isoform-specific manner, i.e., lipo-apoE4>lipo-apoE3 or lipo-apoE2, and thereby further diminished apoE BBB clearance compared with their respective lipid-poor isoforms (Figure 1B). Since lipo-apoE was a mixture of different size particles, i.e., 7–12 nm and 12–17 nm (33), in a separate study, we compared clearance of different size lipo-apoE particles. As illustrated for lipo-apoE3, there was not a significant difference in clearance from the brain between 7–12 nm and 12–17 nm particles compared with a mixture of 7–17 nm particles (Supplemental Figure 1; supplemental material available online with this article; doi:10.1172/JCI36663DS1). Therefore, in all studies with lipo-apoE, we used a mixture of apoE particles.

According to our model (see Methods), the elimination of inulin from brain ISF (Figure 1A) reflects a passive drainage of molecules via the ISF bulk flow, as reported (16, 17, 19). The fractional transport rate constants (k, $min^{-1} \times 10^3$) for different apoE lipid–poor and lipidated isoforms were calculated from 72 individual experiments (as shown in Figure 1A) by using Equations 2 and 4 (see Methods). The rates of the total efflux, elimination via transport across the BBB, elimination by the ISF bulk flow, and retention in the brain corrected for degradation as well as the half-times

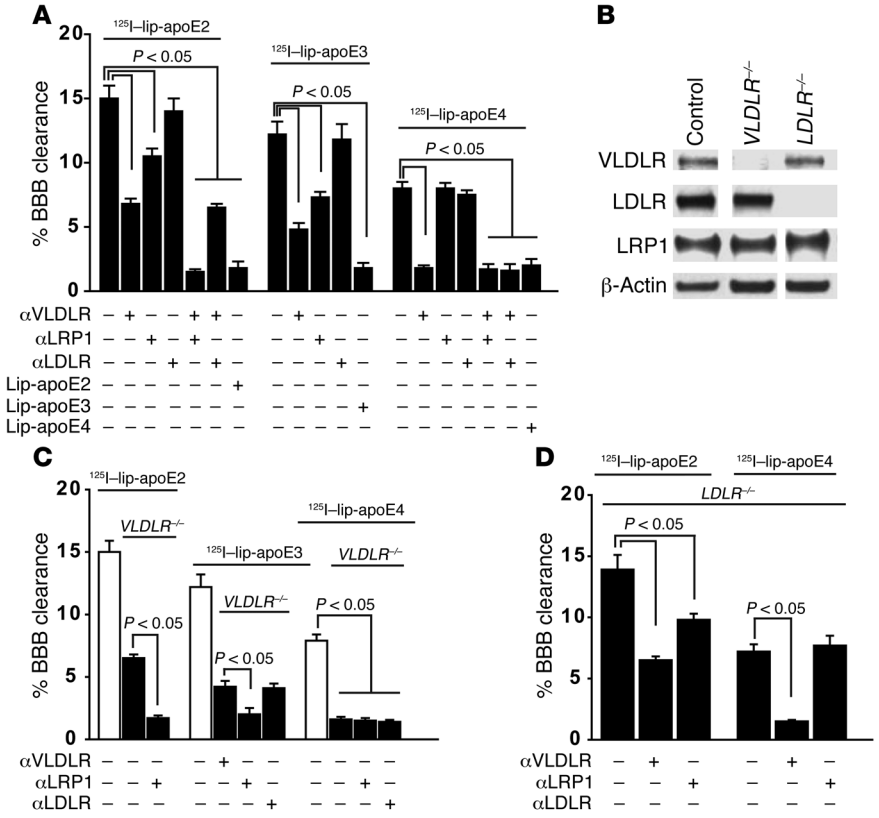

Figure 2
apoE isoform–specific clearance across the mouse BBB in vivo depends on differential contributions of VLDLR-mediated and LRP1-mediated transport. (**A**) ^{125}I-labeled lipo-apoE2, lipo-apoE3, and lipo-apoE4 (TCA-precipitable ^{125}I-radioactivity) BBB clearance at 90 minutes in the presence and absence of receptor-specific blocking antibodies against VLDLR, LRP1, and LDLR and excess unlabeled ligands at 0.5 μM. (**B**) Western blot analysis of VLDLR, LDLR, and LRP1 in brain microvessels isolated from control, *VLDLR*$^{-/-}$, and *LDLR*$^{-/-}$ mice. β-actin was used as a loading control. The lanes were run on the same gel but were noncontiguous. Representative blots from 3 mice per group are shown. (**C** and **D**) ^{125}I-labeled lipo-apoE2, lipo-apoE3, and lipo-apoE4 (TCA-precipitable ^{125}I-radioactivity) BBB clearance at 90 minutes in *VLDLR*$^{-/-}$ (**C**) and *LDLR*$^{-/-}$ mice (**D**) in the presence and absence of receptor-specific antibodies against VLDLR, LRP1, or LDLR. Values are mean ± SEM; n = 3–5 mice per group.

for clearance and retention in the brain are given in Supplemental Table 1. Figure 1B and Supplemental Table 1 show that the transport rate via the BBB of lipo-apoE4 was 8.3-fold, 4.9-fold, and 2.9-fold lower than that for free Aβ40, lipid-poor apoE2 or apoE3, and apoE4, respectively, and 2.6-fold and 2.4-fold lower than for lipo-apoE2 and lipo-apoE3, respectively. Conversely the retention rate of free Aβ40 in the brain was the shortest, i.e., 4.1×10^{-3} min^{-1}, as reported (16). This was 1.7-fold faster than for Aβ42, consistent with the previous report demonstrating a 1.9-fold faster BBB efflux rate for Aβ40 compared with Aβ42 (19). Aβ40 retention rate was 3.8-fold and 9.5-fold less than for lipid-poor apoE2 and apoE4, respectively, or 11.7 and 15.9 times less than for lipo-apoE2 and lipo-apoE4, respectively (Supplemental Table 1). These data indicate that lipo-apoE4 has by far the greatest retention rate in the brain and very slow efflux across the BBB compared with other apoE isoforms or Aβ peptides.

During these relatively short-term transport kinetic experiments, apoE was minimally degraded in the brain ISF at 30 or 300 minutes (less than 10%), as shown by TCA-precipitation and SDS-PAGE analyses of brain tissue supernatants after ^{125}I-apoE2 and ^{125}I-apoE4 microinfusion (Supplemental Figure 2, A and B). However, there was a significant time-dependent progressive degradation of both apoE2 and apoE4 in plasma, as shown by a significant increase in their respective TCA nonprecipitable fractions (Supplemental Figure 2C), indicating metabolism either during transport across the BBB and/or during systemic clearance in the circulation. There was also very low degradation of lipo-apoE isoforms ranging from 10%–15%, as indicated by the TCA-precipitation analysis of brain supernatants after ^{125}I–lipo-apoE2 and ^{125}I–lipo-apoE4 microinfusion (Supplemental Figure 2D). The relative contributions to clearance of apoE isoforms by transport across the BBB, ISF flow and degradation, and retention in the brain of undegraded and uncleared apoE ligands indicated a reciprocal relationship between transport across the BBB and retention of apoE ligands in the brain, namely, the higher the BBB transport, the lower the retention in the brain and vice versa (Figure 1C). The slow clearance via the ISF flow and low rates of degradation were similar between different lipid-poor and lipo-apoE isoforms and did not influence significantly BBB transport or retention. This analysis importantly suggests that a failure in effective removal across the BBB is a key to high retention of lipo-apoE4 in the brain compared with apoE3 or apoE2, which exhibit moderate transport across the BBB.

All 3 lipid-poor apoE isoforms (Figure 1D) as well as lipo-apoE isoforms (not shown) appeared in the cerebrospinal fluid (CSF) with a pattern comparable to that of inulin, a reference molecule that is cleared from brain ISF into CSF by passive diffusion via ISF bulk flow (16). Therefore, apoE clearance from brain ISF to CSF did not exhibit an isoform-specific effect. In contrast, apoE isoforms microinjected into brain ISF appeared in plasma with a significantly different pattern, i.e., apoE2 and apoE3 greater than apoE4 (TCA precipitable), compared with almost negligible levels of inulin at the corresponding time points between 100 and 300 minutes (Figure 1E). These data confirmed that (a) the reference molecule inulin is not transported across the BBB, as shown previously (16, 19, 34), (b) there is an in vivo transcytosis of apoE2 and apoE3 across the BBB into the blood, and (c) apoE4 transport across the BBB from brain to blood is negligible. It is of note that the time-appearance curves of apoE isoforms in plasma cannot be used to estimate total recovery of

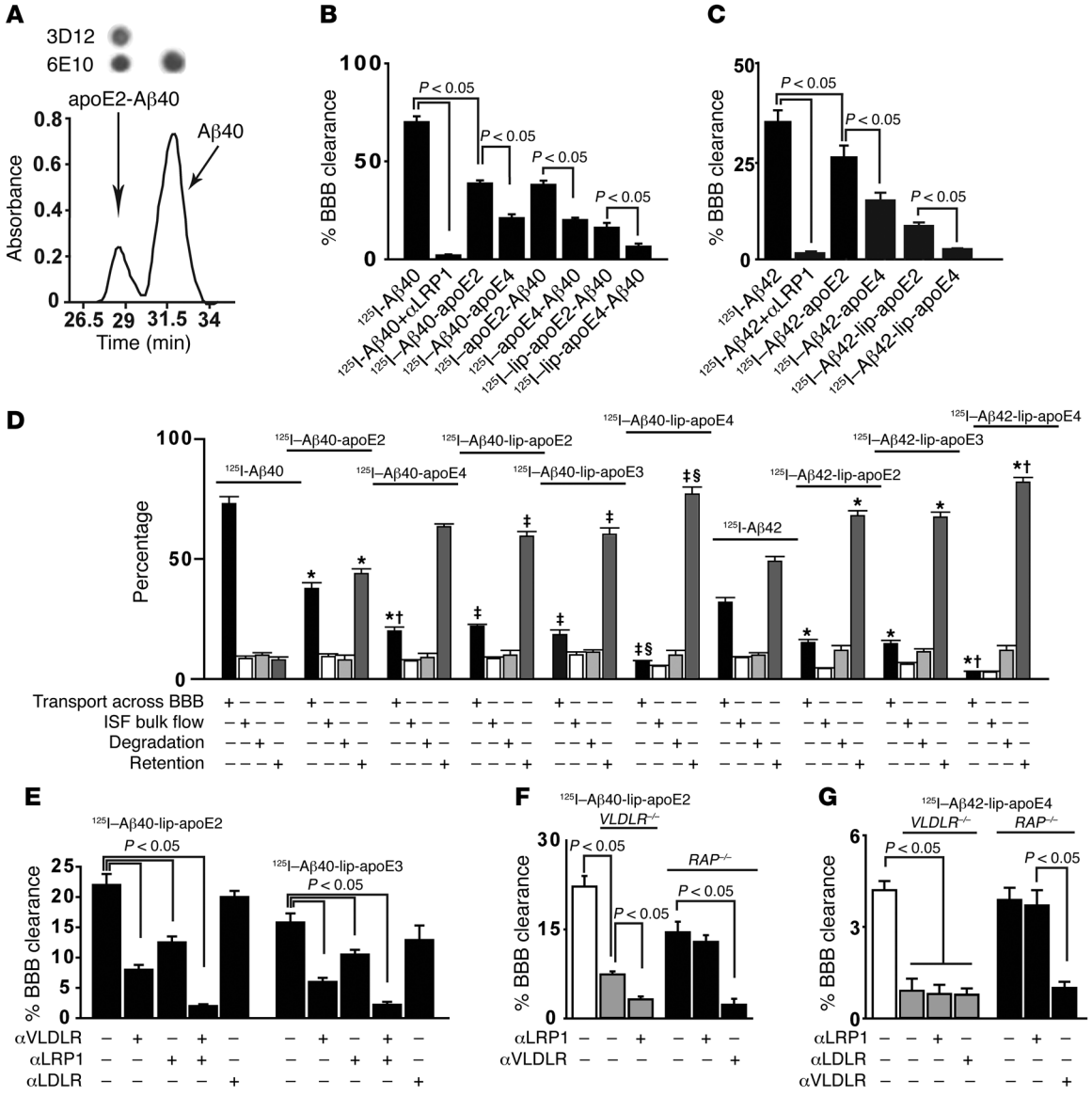

Figure 3

apoE isoforms disrupt Aβ clearance across the mouse BBB in vivo (apoE4>apoE3 or apoE2) by redirecting differentially redirecting transport of Aβ-apoE complexes from LRP1 to VLDLR. ^{125}I-labeled apoE-Aβ complexes (40 nM) and ^{14}C-inulin were microinfused into brain ISF and clearance determined at 90 minutes. ^{125}I-label was either on Aβ40 and Aβ42 or on apoE2 and apoE4. (**A**) FPLC purification of apoE2-Aβ40. Upper panel shows dot blots of Aβ40-apoE2 and free Aβ peaks with Aβ-specific (6E10) and apoE-specific (3D12) antibodies. (**B** and **C**) BBB clearance of Aβ40 (**B**) and Aβ42 (**C**) with and without an LRP1-specific blocking antibody and of their complexes with lipid-poor and lipo-apoE2 and lipid-poor and lipo-apoE4, as indicated. (**D**) Clearance of Aβ40 and Aβ42 by transport across the BBB (black bars), ISF flow (white bars) and degradation (light gray bars) and retention in the brain (dark gray bars) studied from different ^{125}I-Aβ40-apoE and Aβ42-apoE complexes at 40 nM and compared with free Aβ40 or Aβ42. ^{125}I-label was on Aβ. Clearance and retention were calculated from fractional coefficients using Equations 2, 5, and 6 (see Methods). Mean ± SEM, n = 5–6 mice per group in a single time-point series. *P < 0.05, Aβ40-apoE2 and Aβ40-apoE4 versus Aβ40 and Aβ42–lipo-apoE2, Aβ42–lipo-apoE3, and Aβ42–lipo-apoE4 versus Aβ42; †P < 0.05, Aβ40-apoE4 versus Aβ40-apoE2 and Aβ42–lipo-apoE4 versus Aβ42–lipo-apoE3 or Aβ42–lipo-apoE2; ‡P < 0.05, Aβ40–lipo-apoE2 and Aβ40–lipo-apoE4 versus Aβ40-apoE2 and Aβ40-apoE4; §P < 0.05, Aβ40–lipo-apoE4 versus Aβ40–lipo-apoE3 or Aβ40–lipo-apoE2. (**E**) BBB clearance of ^{125}I-Aβ40–lipo-apoE2 and ^{125}I-Aβ40–lipo-apoE3 in control mice with and without blocking antibodies to VLDLR, LRP1, and LDLR. (**F** and **G**) BBB clearance of ^{125}I-Aβ40–lipo-apoE2 (**F**) and ^{125}I-Aβ42–lipo-apoE4 complexes (**G**) in control (white bars), *VLDLR*$^{-/-}$ (gray bars), and *RAP*$^{-/-}$ (black bars) mice with and without blocking antibodies to LRP1, VLDLR, and/or LDLR. Mean ± SEM; n = 4–6 mice per group.

apoE ligands in plasma because apoE entering the plasma compartment is continuously removed from the plasma by systemic clearance via liver, kidney, and other organs (19). Therefore, the areas under curves in Figure 1E underestimate apoE recovery in plasma. Similarly, the time-appearance curves of apoE in the CSF are influenced by the CSF's rapid turnover rate, which continuously clears molecules into blood by nonspecific absorption across the arachnoid granulations (2).

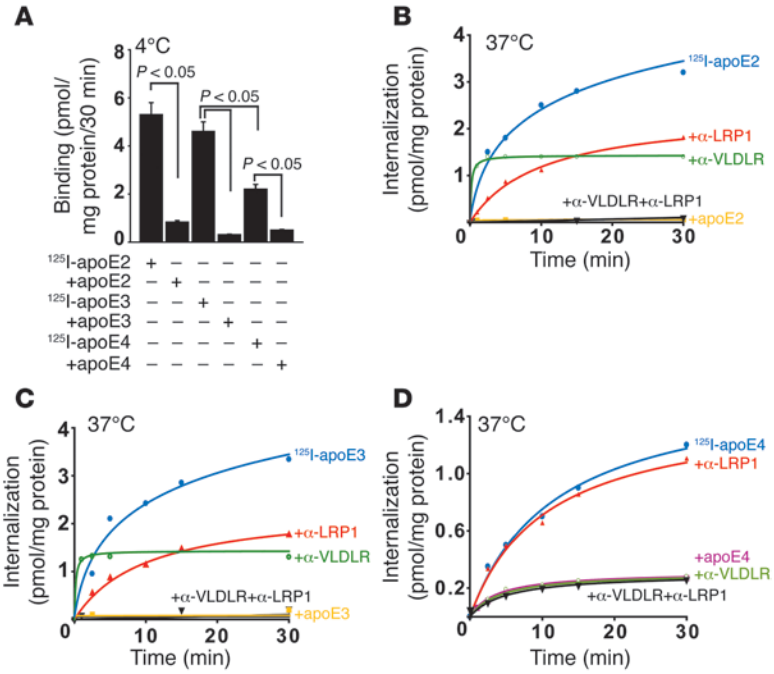

Figure 4
Isoform-specific lipid-poor apoE clearance at the abluminal surface of mouse brain capillaries in vitro is regulated by differential internalization rates of VLDLR and LRP1. (**A**) Specific binding of ^{125}I-labeled lipid-poor apoE2, apoE3, and apoE4 (2 nM, TCA-precipitable ^{125}I-radioactivity) by brain microvessels studied for a period of 30 minutes at 4°C with and without excess of unlabeled ligand at 0.5 μM. (**B**–**D**) Time-dependent internalization of lipid-poor ^{125}I-apoE2 (**B**), ^{125}I-apoE3 (**C**), and ^{125}I-apoE4 (**D**) on the abluminal surface of brain microvessels in the presence of receptor-specific blocking antibodies to LRP1 and VLDLR and excess of unlabeled ligand at 0.5 μM.

Since apoE binds to different lipoprotein receptors, e.g., VLDLR, LDL receptor (LDLR), and LRP1 (35) that are expressed at the BBB and may have roles in signaling, endocytosis, and/or transcytosis of their respective ligands (36), we next used lipoprotein receptor–specific antibodies (Fab_2) against VLDLR, LDLR, and LRP1 to determine whether blocking these receptors influences the efflux of apoE isoforms across the BBB. Specific receptor–blocking antibodies were infused in the ISF 15 minutes prior to tracer infusion and then simultaneously with the tracer mixture containing test apolipoproteins at their physiologic CSF concentration of 40 nM. Figure 2A shows that anti-VLDLR– and anti-LRP1–blocking antibodies inhibited the BBB efflux of lipo-apoE2 and lipo-apoE3 by 50% and 30%, and 58% and 40%, respectively, while anti-LDLR did not have an effect. A combination of anti-VLDLR and anti-LRP1 almost completely (~85%) inhibited apoE2 efflux at the BBB, whereas adding anti-LDLR to anti-VLDLR did not have an effect on apoE2 efflux inhibition greater than that of adding anti-VLDLR alone. The BBB clearance of both lipo-apoE2 and lipo-apoE3 was almost completely inhibited (>90%) by excess unlabeled ligand. These data suggest that VLDLR and LRP1 are likely to have a role in mediating apoE2 and apoE3 efflux at the BBB, whereas a nonspecific clearance accounts for less than 10% of the specific receptor–mediated clearance. In contrast, blocking LRP1 or LDLR did not have an effect on lipo-apoE4 efflux at the BBB (Figure 2A), whereas blocking VLDLR resulted in more than 85% inhibition. Adding anti-LRP1 or anti-LDLR to anti-VLDLR did not result in greater inhibition of lipo-apoE4 efflux compared with inhibition seen with adding anti-VLDLR alone. As with apoE3 and apoE2, excess unlabeled ligand inhibited ^{125}I–lipo-apoE4 clearance by more than 85%. These data suggest that VLDLR is a major receptor mediating lipo-apoE4 efflux at the BBB, whereas LRP1 is not involved. A minor portion (~10%) of BBB apoE4 clearance was by a nonspecific unsaturable transport, as with apoE2 and apoE3. A similar pattern for the receptors' involvement was obtained with lipid-poor apoE2 and apoE4 (Supplemental Figure 3), suggesting VLDLR and LRP1 are required for efflux of apoE2 across the BBB, whereas VLDLR, but not LRP1, mediates very slow efflux of apoE4.

The involvement of receptors was next tested using mice with specific deletions of the *VLDLR* and *LDLR* genes. First, we showed that deletion of the *VLDLR* gene does not alter the expression of LDLR and LRP1 proteins in brain capillaries and, similarly, that *LDLR* deletion does not alter the expression of VLDLR and LRP1 in brain capillaries (Figure 2B). Deletion of the *VLDLR* gene, however, reduced clearance of lipo-apoE2 and lipo-apoE3 by about 60% and clearance of lipo-apoE4 at the BBB by more than 80% (Figure 2C). Addition of an LRP1-specific blocking antibody led to an approximately 90% inhibition of apoE2 and apoE3 BBB efflux in *VLDLR*$^{-/-}$ mice compared with values in the wild-type mice (Figure 2C) but did not have an effect on lipo-apoE4 efflux (Figure 2C). These data confirmed that VLDLR is a major receptor for apoE4 clearance from brain, whereas both LRP1 and VLDLR clear apoE2 and apoE3 at the BBB. We performed a similar experiment in *LDLR*$^{-/-}$ mice and found that deletion of LDLR did not affect either lipo-apoE2 or lipo-apoE4 efflux at the BBB (Figure 2D). The addition of VLDLR and LRP1 antibodies decreased efflux of lipo-apoE2 in *LDLR*$^{-/-}$ mice by 58% and 32%, thus confirming the role of these 2 receptors in apoE2 clearance. Conversely, blocking LRP1 did not have any effect on lipo-apoE4 efflux in *LDLR*$^{-/-}$ mice, whereas VLDLR-specific antibodies diminished efflux of lipo-apoE4 by 85%, confirming that VLDLR is a major receptor required for slow apoE4 clearance at the BBB.

Since apoE binds Aβ with high affinity and is known to be an Aβ-binding protein (21), we next determined whether binding of Aβ to apoE alters Aβ clearance across the BBB from preformed apoE-Aβ complexes. The formation of apoE2-Aβ40 and apoE4-Aβ40 complexes was demonstrated by 4%–20% Tris-glycine nondenaturing gradient gel electrophoresis for lipidated complexes and 10%–20% Tris-tricine native PAGE analysis for lipid-poor complexes (not shown), as we reported previously (33, 37).

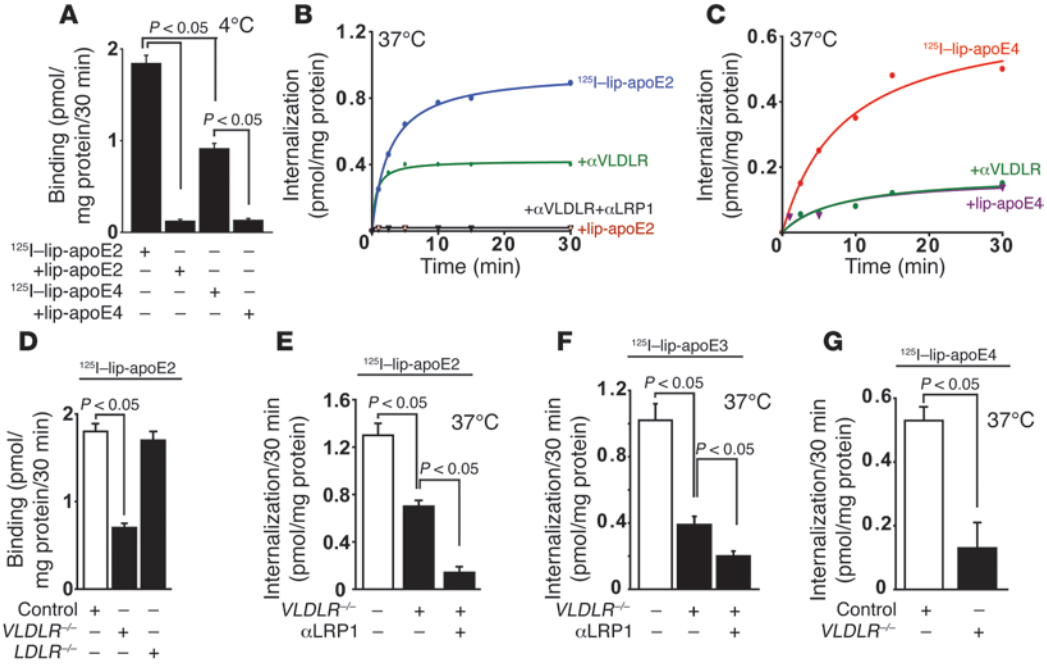

Figure 5

Isoform-specific lipo-apoE clearance at the abluminal surface of mouse brain capillaries in vitro is regulated by differential internalization rates of VLDLR and LRP1. (**A**) Binding of ^{125}I-labeled lipo-apoE2 and lipo-apoE4 (2 nM, TCA-precipitable ^{125}I-radioactivity) to isolated brain microvessels. (**B** and **C**) Time-dependent internalization of ^{125}I-labeled lipo-apoE2 (**B**) and lipo-apoE4 (**C**) in the presence of receptor-specific blocking antibodies against VLDLR and LRP1 and excess of unlabeled ligand at 0.5 μM. (**D**) Binding of ^{125}I-labeled lipo-apoE2 to brain microvessels from control, *VLDLR*$^{-/-}$, and *LDLR*$^{-/-}$ mice. (**E**–**G**) Internalization of ^{125}I-labeled lipo-apoE2 (**E**), lipo-apoE3 (**F**), and lipo-apoE4 (**G**) at the abluminal surface of brain microvessels from control (white bars) and *VLDLR*$^{-/-}$ (black bars) mice studied for a period of 30 minutes. Means ± SEM, n = 3 experiments per group.

Size exclusion chromatography was used to remove excess free Aβ from all apoE-Aβ preparations. For example, in the case of a lipid-poor apoE2-Aβ40 complex, a peak eluting at 29 minutes that was positive for both apoE (3D12 antibody) and Aβ (6E10) represented an Aβ40-apoE complex (Figure 3A), whereas excess free Aβ eluted later with a peak at 32 minutes that was positive only for 6E10 (Aβ) and negative for 3D12 (apoE), indicating free Aβ. We then compared clearance of free Aβ40 versus Aβ40-apoE complexes with either apoE2 or apoE4 at equimolar physiologic CSF concentrations (40 nM). In contrast to free Aβ40, Aβ-apoE2 or Aβ-apoE4 complex was not cleared significantly at the BBB within 30 minutes (not shown). At 90 minutes, more than 85% of free Aβ40 was eliminated at the BBB exclusively through an LRP1-mediated transport (i.e., blockade or lack of VLDLR and LDLR did not influence Aβ efflux), as reported (16, 17, 19). This clearance was much greater than the approximately 38% and 24% clearance of Aβ40 seen when it was complexed with lipid-poor apoE2 and apoE4, respectively (Figure 3B). The same results were obtained regardless of whether the label (^{125}I) was on apoE or Aβ. apoE lipidation further diminished the BBB efflux of Aβ40 to 15% and 9% via apoE2 and apoE4, respectively. Even more pronounced differences were obtained between Aβ42-apoE2 and Aβ42-apoE4 complexes (Figure 3C). For example, only 25% and 12% of Aβ42 was cleared via lipid-poor apoE2 and apoE4, respectively, whereas 9% and 3% of Aβ42 was cleared by lipo-apoE2 and lipo-apoE4, respectively, compared with 38% as seen for free unbound Aβ42.

As we reported, there was minimal degradation of free monomeric Aβ40 or Aβ42 microinjected into the brain ISF (16, 17). In these relatively short-term kinetic studies and at apoE levels corresponding to physiological concentrations of apoE in the CSF, degradation of Ab was not significantly influenced by its binding to either apoE2, apoE3, or apoE4 (either lipid poor or lipidated) at 30 and 300 minutes. Degradation of both Aβ40 and Aβ42 was approximately 10% (Supplemental Figure 2, E and F; Figure 3D). Figure 3 D shows the relative contributions of transport across the BBB, ISF flow, and degradation to the clearance of Aβ40 and Aβ42 when in complex with apoE2, apoE3, or apoE4 isoforms compared with free Aβ40 and Aβ2. The data indicate that binding of Aβ to apoE inhibits rapid efflux of Aβ40 and Aβ42 across the BBB in an isoform-specific fashion, i.e., Aβ clearance was inhibited to the greatest degree when in complex with apoE4 compared with clearance of Aβ-apoE3 and Aβ-apoE2, and this inhibition was significantly enhanced by apoE lipidation. There was a reciprocal relationship between reductions in BBB transport and accumulations of undegraded Aβ-apoE complexes in the brain, whereas the ISF flow and degradation were similar for all studied complexes. Aβ40 and Aβ42 efflux across the BBB was inhibited to the greatest degree when either was complexed with lipo-apoE4; efflux was 3-fold lower for such complexes compared with Aβ complexed with lipo-apoE3 or lipo-apoE.

We next used a panel of lipoprotein receptor–specific antibodies to determine whether the same receptors mediating apoE2, apoE3, and apoE4 efflux at the BBB are required for efflux of Aβ complexes with apoE2, apoE3, and apoE4. Clearance of ^{125}I-Aβ40–lipo-apoE2 and ^{125}I-Aβ40–lipo-apoE3 complexes at the BBB was inhibited by both VLDLR and LRP1 antibodies (Figure 3E); the involvement of

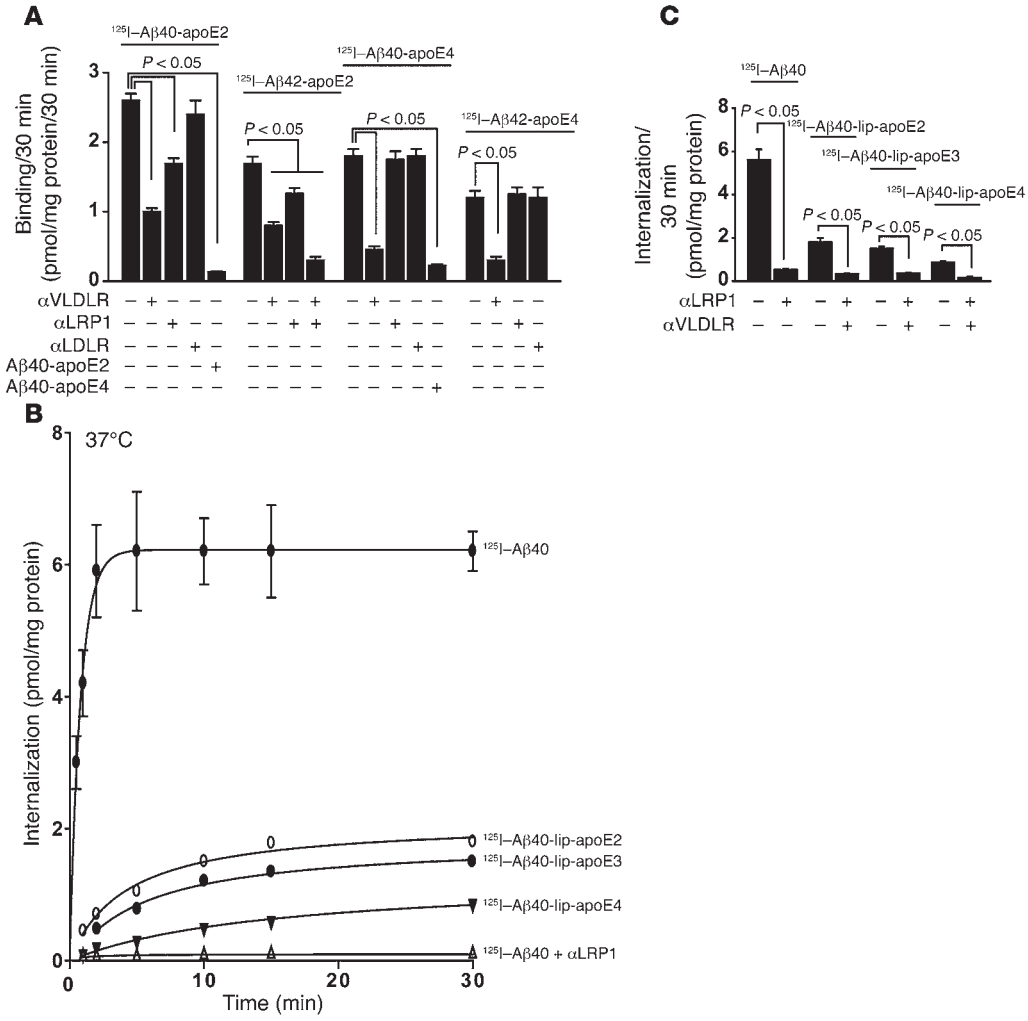

Figure 6
apoE isoform–specific inhibition (apoE4>apoE3 and apoE2) of Aβ internalization at the abluminal surface of mouse brain capillaries in vitro is mediated by VLDLR. (**A**) Specific binding of ^{125}I-labeled Aβ40 and Aβ42 complexes with apoE2 and apoE4 at 4°C in the absence and presence of receptor-specific blocking antibodies to VLDLR, LDLR, or LRP1 and excess unlabeled ligand at 0.5 μM. (**B**) Internalization of ^{125}I-Aβ40 in the absence and presence of receptor-specific blocking antibodies against LRP1 and of ^{125}I-labeled Aβ40–lipo-apoE2, Aβ40–lipo-apoE3, and Aβ40–lipo-apoE4 complexes for a period of 30 minutes. (**C**) Internalization of ^{125}I-labeled Aβ40, Aβ40–lipo-apoE2, Aβ40–lipo-apoE3, and Aβ40–lipo-apoE4 in the absence and presence of receptor-specific blocking antibodies against LRP1 and VLDLR. Means ± SEM; n = 3–5 experiments per group.

VLDLR was confirmed in *VLDLR*$^{-/-}$ mice, which exhibited a 60% reduction in ^{125}I-Aβ40–lipo-apoE2 clearance compared with littermate controls (Figure 3F). As seen with apoE2, anti-LRP1 inhibited the efflux of ^{125}I-Aβ40–lipo-apoE2 from brains in *VLDLR*$^{-/-}$ mice by an additional 30%. In contrast, ^{125}I-Aβ42–lipo-apoE4 BBB clearance was inhibited by more than 80% in *VLDLR*$^{-/-}$ mice compared with controls and was not affected by an LRP1-specific antibody (Figure 3G). Efflux of ^{125}I-Aβ40–lipo-apoE2 was significantly reduced (by approximately 40%) in *RAP*$^{-/-}$ mice (Figure 3F), a functional LRP1 knockout with severely depleted (~80%) LRP1 levels at the BBB (17). In contrast, ^{125}I-Aβ40–lipo-apoE4 efflux at the BBB was not affected in *RAP*$^{-/-}$ mice (Figure 3G). These experiments confirm the results obtained with LRP1-specific blocking antibodies.

We then asked whether isoform-specific differences in apoE clearance across the BBB in vivo may reflect differences among the internalization rates of different apoE isoforms by their respective lipoprotein receptors at the abluminal side of the BBB. To address this question, we used isolated mouse brain microvessels as a model, as reported (17). Lipid-poor apoE bound to the abluminal surfaces of isolated mouse brain microvessels in an isoform-specific manner, e.g., apoE2>apoE3>apoE4, and was almost displaced by excess unlabeled ligand (Figure 4A). Receptor-bound apoE2 and apoE3 were internalized by endocytosis with a $t_{1/2}$ of about 3.9 ± 0.3 and 3.6 ± 0.4 minutes, respectively (Figure 4, B and C). Specific lipoprotein receptor–blocking antibodies were then used to identify the respective contributions of VLDLR and LRP1 in apoE2 and apoE3 endocytosis. First, we showed that apoE2 internalization was inhibited completely when both VLDLR and LRP1 were blocked as well as when there was excess unlabeled apoE2 (Figure 4B). When VLDLR only was blocked, apoE2 internalization reflected endocytosis via LRP1 that was extremely rapid, with a $t_{1/2}$ of less than 30 seconds, consistent with the previously shown rapid endocytic rate of LRP1 (17, 32). In contrast, when LRP1 was blocked, the apoE2 internalization was much slower, with a $t_{1/2}$ of 8.5 ± 1.5 minutes. This is consistent with a previous study demonstrating that VLDLR has the slowest internalization rate of all lipoprotein receptors (32). Similar results suggesting a rapid efflux component via LRP1 and a slow efflux component via VLDLR were obtained for apoE3 (Figure 4C). We next repeated the same experiment with apoE4 and found that its internalization rate was much slower than that of apoE2 and apoE3, with a $t_{1/2}$ of 8.7 ± 1.5 minutes (Figure 4D). Blockade of VLDLR resulted in almost complete inhibition of apoE4 internalization, whereas blockade of LRP1 did not affect apoE4 endocytosis, consistent with our in vivo findings. LRP1- and VLDLR-specific antibodies together did not have a greater effect on inhibition of apoE4

internalization than VLDLR antibody alone. Therefore, in the presence of an LRP1 antibody, apoE4 endocytosis was mediated via VLDLR, with a $t_{1/2}$ of 8.9 ± 1.3 minutes, which was comparable to a $t_{1/2}$ of VLDLR-mediated internalization for the Aβ-apoE2 and Aβ-apoE3 complexes. These results suggest that LRP1 contributed to a substantially faster internalization rate at the BBB of apoE2 and apoE3 compared with apoE4, which was internalized slowly by VLDLR only. During these short-term kinetic internalization studies, there was low degradation (<5%) of apoE2 and apoE4, as determined by their respective TCA nonprecipitable fractions in brain vessel lysates and in the incubation medium over the studied short periods of time (not shown).

Next, we used astrocyte-derived lipo-apoE particles to determine whether the same internalization receptor requirements held as for the lipid-poor apoE isoforms. There was again an isoform-specific difference in lipo-apoE2 versus lipo-apoE4 binding (Figure 5A). The internalization rate of lipo-apoE2 was significantly faster than that of lipo-apoE4 (Figure 5, B and C), with the respective $t_{1/2}$ values of 3.9 ± 0.4 minutes and 8.4 ± 1.4 minutes, which were comparable to the $t_{1/2}$ values of their lipid-poor counterparts (see above). A combination of VLDLR- and LRP1-specific blocking antibodies resulted in complete inhibition of lipo-apoE2 internalization, whereas inhibition of VLDLR revealed a fast LRP1 component of lipo-apoE2 internalization, with a $t_{1/2}$ of less than 30 seconds (Figure 5B). Internalization of lipo-apoE4 was almost completely blocked with a VLDLR-specific antibody, revealing no fast LRP1 component, as seen for lipid-poor apoE4 (Figure 5C). By using isolated capillaries from *VLDLR*$^{-/-}$ and *LDLR*$^{-/-}$ mice, we confirmed that LDLR was not involved in uptake of lipo-apoE2 or lipo-apoE4 (not shown), whereas deletion of VLDLR resulted in a greater than 60% reduction in apoE2 binding (Figure 5D) and internalization (Figure 5E) as well as in an approximately 60% inhibition in lipo-apoE3 internalization (Figure 5F). In *VLDLR*$^{-/-}$ mice, the internalization of lipo-apoE2 or lipo-apoE3 was inhibited up to 90% by addition of an LRP1-specific antibody (Figure 5, E and F). Internalization of lipo-apoE4 was inhibited by approximately 80% in *VLDLR*$^{-/-}$ mice (Figure 5G).

Binding and internalization of apoE-Aβ complexes at the abluminal surface of brain microvessels was next studied using the fast protein liquid chromatography–purified (FPLC-purified) apoE2-Aβ40 and apoE4-Aβ40 complexes as above. Aβ40-apoE2 and Aβ42-apoE2 complexes bound to both VLDLR and LRP1, whereas Aβ40-apoE4 and Aβ42-apoE4 complexes bound only to VLDLR, not to LRP1, as shown with the lipoprotein receptor–specific blocking antibodies (Figure 6A). Binding of radiolabeled complexes was inhibited by more than 90% by excess unlabeled ligand. The internalization rate of free Aβ40 was rapid, i.e., $t_{1/2}$ was less than 30 seconds and was completely inhibited by an LRP1-specific antibody, as reported (17). The internalization rates of Aβ40 complexes with lipo-apoE2 and lipo-apoE3 were comparable but substantially lower than for Aβ40 alone, as indicated by their respective internalization curves (Figure 6B). There was a clear isoform-specific effect, i.e., lipo-apoE2 and lipo-apoE3 internalized Aβ40 at rates significantly higher than lipo-apoE4 (Figure 6B). As shown in Figure 6C, both VLDLR and LRP1 were involved in endocytosis of Aβ40 via lipo-apoE2 and lipo-apoE3, whereas VLDLR was the key receptor for internalization of Aβ40–lipo-apoE4 complex. LRP1-dependent internalization of Aβ40 was shown by comparison.

Discussion

APOE genotype is the only established genetic risk factor for late-onset sporadic AD with an isoform-specific risk profile of apoE4>apoE3>apoE2 (21, 38, 39). Still, it remains unclear how apoE4 accelerates and apoE2 retards AD pathology to influence cognitive decline. A number of experimental studies have demonstrated that apoE critically regulates the fate of Aβ in the brain. For example, studies in Aβ precursor protein (APP-expressing) mice have suggested that deletion of mouse *apoE* gene inhibits development of fibrillar amyloid plaques (26). On the other hand, expression of human apoE isoforms in these mice resulted in isoform-dependent and gene-dose–dependent delay in the onset of plaque deposition and decrease in amyloid burden (23). These studies suggest that apoE may regulate in vivo fibrillization of Aβ as well as the levels of soluble Aβ in the brain in an isoform-specific fashion, but the exact molecular mechanism or mechanisms have not been identified.

The present study demonstrates that apoE disrupts clearance of Aβ from brain ISF in an isoform-specific fashion (e.g., apoE4>apoE3 and apoE2). apoE4 shifted BBB efflux of Aβ completely from LRP1-mediated rapid brain capillary transcytosis (16, 17) to a very slow interaction of Aβ-apoE complexes, with VLDLR at the abluminal side of the BBB, resulting in poor Aβ clearance of apoE-Aβ complexes from brain. Lipo-apoE4 increased brain retention of Aβ40 and Aβ42 complexed to apoE4 in mice by 15- and 9-fold, respectively, compared with the unbound peptides. In contrast, apoE2 and apoE3 only moderately inhibited Aβ clearance due to their ability to interact at least partially with LRP1 in addition to VLDLR. Based on the present findings, one may speculate that the virtual blockade of fibrillar Aβ deposition, as seen in apoE-null mice crossed with APP transgenics (26), may at least in part be due to an improved Aβ clearance from brain directly related to a loss of apoE-mediated Aβ retention. Human isoform–specific differences in Aβ accumulation in APP mice crossed with human apoE transgenics and knockin mice on mouse apoE-null background (i.e., apoE4>apoE3>apoE2) (22, 23, 27, 28) might reflect apoE isoform–specific disruption of free Aβ clearance, which is significantly greater with apoE4 than with apoE3 and apoE2. The reason that Aβ deposition occurs earlier in APP transgenic mice on a mouse apoE-null background versus mice expressing human apoE (22, 28, 30) is not clear. However, it must be noted that fibrillar Aβ or true amyloid deposition is delayed to the greatest extent in the absence of apoE, consistent with human apoE isoform–mediated retention of an apoE-bound Aβ pool leading to earlier Aβ fibril formation in an isoform-specific fashion.

In addition to mediating endocytosis and signaling in the vascular wall (40), the lipoprotein receptors mediate transcytosis of their ligands across the BBB (36). For example, LRP2 mediates transport of apoJ and apoJ-Aβ complexes across the BBB (19, 41), LDLR may transport LDL (42) and LDL apoproteins conjugated to nanoparticles encapsulating pharmaceuticals (43) across the BBB, and LRP1 mediates clearance of unbound Aβ across the BBB (16, 17). Earlier work indicated limited BBB permeability to circulating lipid-poor apoE2, apoE3, and apoE4 (37), supporting the concept that apoE in blood and brain are regulated independently (44, 45). Nevertheless, the observed differences in Aβ efflux at the BBB by apoE isoforms may contribute to isoform-specific apoE control of Aβ levels in the brain, which in turn may influence the development of Aβ pathology in AD models and AD.

Our findings showing that VLDLR internalizes Aβ-apoE2, Aβ-apoE3, or Aβ-apoE4 complexes at the BBB with a $t_{1/2}$ that is more than 20-fold shorter than with LRP1-mediated internalization of Aβ-apoE2, Aβ-apoE3, or Aβ is consistent with an earlier report showing that the endocytotic rate of VLDLR is approximately 25-fold slower than that of LRP1 (32). While there have been numerous studies on the interaction of apoE with LDL receptor family members, only a few compare apoE isoform–binding affinities to lipoprotein receptors using the same methods. Recently, by using a solid-phase binding assay, surface plasmon resonance (SPR), and cell uptake experiments, it has been shown that VLDLR does not discriminate between the apoE isoforms and binds and internalizes lipid-free apoE2, apoE3, and apoE4 as well as their corresponding lipidated isoforms (46), which is consistent with the present findings. Although it has been reported that LDLR shows a marked preference for lipo-apoE3 and lipo-apoE4 and binds apoE2 isoform poorly (47), our study revealed that lipid-free or lipo-apoE isoforms do not use LDLR as an efflux receptor at the BBB. This finding is consistent with a concept that LDLR at the BBB acts mainly as an influx but not efflux receptor for LDL particles, thus mediating transport of its ligands in the direction from blood to brain but not from brain to blood (42, 43). However, deletion of LDLR elevates brain and CSF apoE3 and apoE4 but not apoE2 in human apoE-knockin mice (48), suggesting that LDLR plays an important role in apoE clearance in nonvascular brain cells (i.e., astrocytes, microglia, neurons).

Earlier binding studies with LRP1 suggested a requirement for apoE-enriched remnant particles or β-migrating VLDL particles (49). A more recent study has demonstrated that LRP1 binds lipo-apoE isoforms with greater affinity than lipid-free isoforms but does not discriminate between lipo-apoE2, lipo-apoE3, and lipo-apoE4 (46). Others have shown that LRP1 mediates cellular uptake of lipid-poor apoE isoforms in fibroblasts (50) and that lipid-poor apoE3 binds to immobilized soluble LRP1 with higher affinity than lipid-free apoE4 (51), although apoE3 exhibited much lower affinity for sLRP1 compared with Aβ. The differences among various studies might result from differences in apoE preparations. Our present findings suggest that LRP1 mediates BBB clearance of both lipid-poor and lipo-apoE2 and lipo-apoE3 and of their complexes with Aβ but not apoE4. The difference between a previous study suggesting binding of lipo-apoE4 to LRP1 (46) and the current study indicating insignificant apoE4 binding to LRP1 could be due to use of different forms of lipo-apoE particles as, for example, those secreted by primary astrocytes as in the present study (33) versus plasma-derived and/or might reflect differences between in vitro binding assays compared with the lack of interaction with LRP1, as seen in situ at the abluminal side of the mouse BBB. It is also possible that apoE4 has greater affinity to bind to LDLR on cells in the brain or heparan sulfate proteoglycans in the extracellular matrix, which precludes its effective interaction with the clearance LRP1 receptor at the BBB.

Lipidation greatly reduced the amount of apoE and its complexes with Aβ that were cleared at the BBB. Although it did not significantly change the $t_{1/2}$ for ligand internalization, lipo-apoE interacts with Aβ in vitro with a higher affinity than its lipid-poor counterparts (52–54). Thus, it is likely that lipidation critically influences both Aβ transport and metabolism. It has been reported that apoE facilitates Aβ degradation by astrocytes (55, 56) and by microglia (57). Recently, it has been demonstrated that endocytic degradation of Aβ peptides within microglia by neprilysin and related enzymes is dramatically enhanced by apoE as well as Aβ degradation by insulin-degrading enzyme (25). The capacity of apoE to promote degradation was isoform dependent (e.g., apoE4<apoE3 or apoE2) and enhanced by expression of lipo-apoE. In contrast to studies showing apoE-mediated cellular clearance of Aβ by astrocytes and microglia (25, 55–57), a lack of significant cellular Aβ degradation from apoE-Aβ complexes in the present study may reflect a relatively smaller role for cellular clearance by astrocytes and microglia of soluble apoE and Aβ when studied in vivo, as detected by microdialysis or in this type of brain clearance study, as we reported (17–19, 34, 58). The isoform-specific brain retention of apoE and apoE-Aβ complexes (apoE4>apoE2 or apoE3) found in the present study might contribute to apoE isoform–specific effects on Aβ cytotoxicity (59), aggregation, and fibrillogenesis (23, 29) as well as apoE self aggregation and neurotoxicity (60).

In summary, our findings suggest that the differences in Aβ clearance from brain by different apoE isoforms might contribute to the observed effects of apoE genotype on the disease process in AD and AD models. As suggested, disrupting Aβ interaction with apoE holds a therapeutic potential for AD (61–64). Considering the present results, such therapies should be able to enhance Aβ clearance from brain.

Methods

Aβ peptides. Aβ40 and Aβ42 were obtained from the W.M. Keck Foundation Biotechnology Resource Laboratory (Yale University, New Haven Connecticut, USA). They were synthesized by solid-phase F-moc (9-fluorenylmethoxycarbonyl) amino acid chemistry, purified by reverse-phase HPLC, and structurally characterized. Lyophilized peptides were kept at –80°C until used.

Proteins. Recombinant lipid-poor human apoE2, apoE3, and apoE4 isoforms from baculovirus-transfected Sf9 cells were purchased from Invitrogen. Lipo-apoE2, lipo-apoE3, and lipo-apoE4 isoforms were prepared and purified from conditioned medium of immortalized mouse astrocytes derived from apoE2-, apoE3-, and apoE4-knockin mice, as previously described (33). These particles were similar in size and cholesterol content to those secreted by primary astrocytes and bind Aβ peptides in physiological buffers (33).

Antibodies. We used polyclonal goat receptor–specific blocking antibodies raised against the extracellular domain of LDLR (AF2255; R&D Systems), VLDLR (AF2258; R&D Systems), and LRP1 (N20; Santa Cruz Biotechnology Inc.).

Radioiodination. Aβ was iodinated with ^{125}I using the lactoperoxidase method (65). The resulting components were resolved by HPLC and the purity analyzed by MALDI-TOF mass spectrometry, as we reported (66). In our studies, we used only reduced monoidinated Aβ peak (specific activity ~60 μCi/μg), as confirmed by MALDI-TOF mass spectrometry analysis, as reported (66). Lipid-poor and lipo-apoE was radiolabeled by IODO-GEN (Thermo Scientific) to a specific activity of 9–12 μCi/μg. Free iodide was removed from radiolabeled apoE preparations by gel filtration.

Formation of Aβ-apoE complexes with monomeric Aβ species. Lipidated and lipid-poor ^{125}I-labeled apoE2 and apoE4 complexes with synthetic human Aβ40 and Aβ42 were prepared as we described (36), except the ratio of Aβ to apoE was 40 to 1. Complexes were purified by fast flow size-exclusion chromatography (FPLC) to remove excess free Aβ. Formation of complexes between lipo-apoE and lipid-poor apoE isoforms with Aβ isoforms and complete removal of excess free Aβ were verified as we reported by nondenaturing 4%–20% Tris-glycine polyacrylamide gel (Invitrogen) (33) and 10%–20% Tris-tricine polyacrylamide gel (Bio-Rad), respectively, followed by Western blot analysis for apoE and Aβ (33). ^{125}I-labeled Aβ40 or Aβ42 complexes with unlabeled apoE2 and apoE4 were also prepared in the same way as described above.

Brain clearance studies. Male mice on a C57BL/6 background weighing 25–27 g and 2 to 3 months old were obtained from The Jackson Laboratory. Mice were kept under standard housing conditions and feeding schedules until the experimental procedures were performed. All studies were performed according to the NIH guidelines using a protocol approved by the University of Rochester Committee on Animal Resources. In brief, a stainless steel guide cannula was implanted stereotaxically into the right caudate putamen of anesthetized mice (100 mg/kg ketamine and 10 mg/kg xylazine i.p.) with the cannula tip coordinates 0.9 mm anterior and 1.9 mm lateral to the bregma and 2.9 mm below the surface of the brain. Clearance studies were performed after animals recovered from surgery. The experiments were performed before substantial chronic process occurred, as assessed by histological analysis of tissue, i.e., negative staining for astrocytes (glial fibrillar acidic protein) and activated microglia (antiphosphotyrosine), but allowed time for BBB repair for large molecules, as reported previously (17, 19, 34, 58).

Injection of tracers mixture. The amount of injected tracers was accurately determined using a micrometer to measure the linear displacement of the syringe plunger in the precalibrated microsyringe. Mock CSF (0.5 μl) containing ^{125}I-labeled test-tracers Aβ (monomer), apoE (lipid poor or lipidated), or Aβ-apoE complex together with ^{14}C-inulin (reference molecule) was microinfused into brain ISF over 5 minutes. When the effects of different unlabeled molecular reagents were tested, they were injected 15 minutes prior to radiolabeled ligands and then simultaneously with radiolabeled ligands, as described (17).

Tissue sampling. At the end of the experiments, brain, blood, and CSF were sampled and prepared for radioactivity analysis and TCA and SDS-PAGE analyses to determine the molecular forms of test tracers (16, 34). Our earlier studies with ^{125}I-labeled Aβ have demonstrated that both radiolabeled Aβ40 and Aβ42 remain mainly intact in brain ISF (>95%) within 30–300 minutes of in vivo clearance studies (16) as well as during short-term kinetic clearance studies in vitro on brain capillaries (17). In the present study, we confirmed previous findings indicating that molecular forms of transport of ^{125}I-labeled Aβ and apolipoproteins within 30–300 minutes of clearance studies remained mainly in their original form of intact molecules, as injected in the CNS.

Calculations of clearance rates. All calculations of clearance parameters were as reported (16, 17, 19). In brief, the percentage of radioactivity of test ligand remaining in the brain after microinfusion was determined as follows:

$$\% \text{ recovery in brain} = 100 \times (N_b/N_i) \quad \text{(Equation 1)}$$

where N_b is the radioactivity of undegraded test ligand remaining in the brain at the end of the experiment and N_i is the radioactivity injected into the brain ISF, i.e., the disintegrations per minute (d.p.m.) for ^{14}C-inulin and the counts per minute (c.p.m.) for TCA-precipitable ^{125}I-radioactivity corrected for degradation were used. Inulin was studied as a metabolically inert polar molecule (reference) that is neither transported across the BBB nor retained by the brain; its clearance rate provides a measure of the ISF bulk flow as reported (16, 19) and was calculated as follows:

$$N_b(\text{inulin})/N_i(\text{inulin}) = \exp(-k \text{ inulin} * t) \quad \text{(Equation 2)}$$

where k indicates inulin elimination rate and t indicates time. According to our published model (16, 19), there are 2 possible physiological transport routes of elimination of apoE and Aβ and of their complexes from brain ISF: direct transport across the BBB into the bloodstream and elimination via ISF bulk flow into the CSF and cervical lymphatics. In addition, cellular uptake and subsequent processing (degradation) and proteolytic degradation within the extracellular spaces may take place. The model allows for the possibility that fractions of apoE or Aβ and/or of their complexes are retained in the brain by binding to the cell surface receptors or other chaperone molecules in the extracellular matrix, which may result either in their metabolism (degradation) or retention of undegraded material in the brain.

In a case of multiple time-point efflux series with departure of the later time points from the linear efflux phase, i.e., more than 30 minutes for Aβ peptides and more than 90 minutes for different apoE ligands, the fraction of test tracer(s) remaining in the brain can be expressed as follows:

$$N_b(\text{Aβ or apoE})/N_i(\text{Aβ or apoE}) = a1 + a2e^{-[k(1)]t} \quad \text{(Equation 3)}$$

where $a1 = k2/(k1 + k2)$ and $a2 = k1/(k1 + k2)$, e denotes exponential, and $k1$ and $k2$ denote the fractional coefficients of total efflux from the brain and retention within the brain corrected for degradation, respectively, as reported (16, 17, 19). The fractional rate constant of Aβ or apoE efflux across the BBB was calculated by using the fractional rate coefficient of total efflux of the test Aβ or apoE tracer and the reference molecule (inulin) as follows:

$$k4 = k1 - k(\text{inulin}) \quad \text{(Equation 4)}$$

The MLAB mathematical modeling system (Civilized Software Inc.) was used to fit the compartmental model to the disappearance curves or percentage of recovery data with inverse square weightage. Kinetic constants were obtained by a nonlinear regression curve fitting (GraphPad Prism 3.02; GraphPad Software).

In a case of a single-time point efflux series within the 90 minutes of the linear efflux of different Aβ-apoE complexes, the fraction of Aβ-apoE that remains undegraded in the brain at 90 minutes is related to the injected dose of the Aβ-apoE tracer by the monoexponential equation as we reported (19):

$$N_b(\text{Aβ-apoE})/N_i(\text{Aβ-apoE}) = \exp(-k3 \text{ Aβ-apoE} * t) \quad \text{(Equation 5)}$$

where $k3$ is the total efflux rate of Aβ-apoE complex, N_b is the radioactivity of undegraded Aβ-apoE complex remaining in the brain at the end of the experiment, and N_i is the radioactivity injected into the brain ISF, i.e., TCA precipitable ^{125}I-radioactivity values corrected for degradation were used. The fraction of Aβ-apoE complex cleared via ISF bulk flow was determined by the clearance rate of simultaneously infused reference molecule inulin using Equation 2, as above. The clearance rates of Aβ-apoE complexes across the BBB, $k4$, were calculated as the difference between the total efflux rate and efflux via ISF flow corrected for degradation, as reported (19):

$$k4 = k3 - k(\text{inulin}) \quad \text{(Equation 6)}$$

Binding and internalization of apoE and Aβ test ligands by isolated brain capillaries. Brain microvessels from control and *VLDLR*$^{-/-}$ and *LDLR*$^{-/-}$ mice on a C57BL/6 background were isolated, as we described (67).

Binding studies. For the binding studies, brain capillaries were incubated in 0.5 ml Eppendorf tubes (Protein LoBind Tube; Eppendorf) in the assay buffer (mock CSF containing 1 mM sodium perchlorate to block free iodide uptake) with ^{125}I-labeled test ligands Aβ40 and Aβ42, apoE2 and apoE4 isoforms (lipid poor and lipidated), and different Aβ-apoE complexes at a concentration of 2 nM at 4°C for 30 minutes, as reported (17). After 30 minutes, the assay buffer containing unbound ligand was removed and capillaries were washed in ice-cold assay buffer and counted. Inhibition studies were performed with polyclonal goat receptor–specific blocking antibodies (60 μg/ml) raised against the extracellular domain of LDLR (AF2255; R&D Systems), VLDLR (AF2258; R&D Systems), and LRP1 (N20; Santa Cruz Biotechnology Inc.). Binding of radiolabeled test ligands to brain capillaries was corrected for the distribution of ^{14}C-inulin

(extracellular space marker) and nonspecific binding and determined as the tissue to medium ratio: c.p.m. for TCA-precipitable ^{125}I-radioactivity (mg capillary protein)/c.p.m. for TCA-precipitable ^{125}I-radioactivity (ml medium) times ligand concentration in the medium (17).

Internalization studies. For the internalization studies, capillaries were incubated in Eppendorf tubes in the assay buffer with 2 nM test ligands at 4°C for 30 minutes in the presence or absence of receptor-blocking antibodies, as described above. After 30 minutes, the assay buffer containing unbound ligand was removed and capillaries were washed once with cold assay buffer, resuspended in prewarmed (37°C) assay buffer, and placed in a 37°C water bath. At predetermined times of 30 seconds and 1, 2.5, 5, 10, 15, and 30 minutes, Eppendorf tubes were quickly placed on ice and incubated for 12 minutes with the ice-cold stop/strip solution to remove ligand from the capillary abluminal cell surface. Capillaries were separated by centrifugation and the capillary pellet was lysed with SDS buffer and counted. The sum of internalized ligand plus the ligand associated with the abluminal cell surface represented the amount of ligand available for internalization (17). The fraction of ligand internalized at each time point was plotted as described (32).

Statistics. Data were analyzed by multifactorial analysis of variance and 2-tailed Student's *t* test. The differences were considered to be significant at $P < 0.05$. All values were mean ± SEM.

Acknowledgments

The authors want to thank the NIH for grants R37 NS34467 and R37 AG023084 (to B.V. Zlokovic) and R37 AG13956 (to D.M. Holtzman).

Received for publication July 2, 2008, and accepted in revised form October 8, 2008.

Address correspondence to: Berislav V. Zlokovic, Kornberg Medical Research Building, Room G-9613, University of Rochester Medical School, 601 Elmwood Avenue, Box 670, Rochester, New York 14642, USA. Phone: (585) 273-3132; Fax: (585) 273-3133; E-mail: Berislav_zlokovic@urmc.rochester.edu.

Rashid Deane and Abhay Sagare contributed equally to this work.

1. Iadecola, C. 2004. Neurovascular regulation in the normal brain and in Alzheimer's disease. *Nat. Rev. Neurosci.* **5**:347–360.
2. Zlokovic, B.V. 2008. The blood-brain barrier in health and chronic neurodegenerative disorders. *Neuron.* **57**:178–201.
3. Rovelet-Lecrux, A., et al. 2006. *APP* locus duplication causes autosomal dominant early-onset Alzheimer disease with cerebral amyloid angiopathy. *Nat. Genet.* **38**:24–26.
4. Hardy, J. 2006. A hundred years of Alzheimer's disease research. *Neuron.* **52**:3–13.
5. Deane, R., Sagare, A., and Zlokovic, B.V. 2008. The role of the cell surface LRP and soluble LRP in blood-brain barrier Aβ clearance in Alzheimer's disease. *Curr. Pharm. Des.* **14**:1601–1605.
6. Lee, V.M.Y., Balin, B.J., Otvos, L., Jr., and Trojanowski, J.Q. 1991. A68: A major subunit of paired helical filaments and derivatized forms of normal tau. *Science.* **251**:675–678.
7. SantaCruz, K., et al. 2005. Tau suppression in a neurodegenerative mouse model improves memory function. *Science.* **309**:476–481.
8. Tanzi, R.E. 2005. The synaptic Abeta hypothesis of Alzheimer disease. *Nat. Neurosci.* **8**:977–979.
9. Snyder, E.M., et al. 2005. Regulation of NMDA receptor trafficking by amyloid-β. *Nat. Neurosci.* **8**:1051–1058.
10. Selkoe, D.J. 2001. Clearing the brain's amyloid cobwebs. *Neuron.* **32**:177–180.
11. Holtzman, D.M., and Zlokovic, B.V. 2007. Role of Aβ transport and clearance in the pathogenesis and treatment of Alzheimer's disease. In *Alzheimer's disease: advances in genetics, molecular and cellular biology*. S. Sisodia, and R.E. Tanzi, editors. Springer. New York, New York, USA. 179–198.
12. Haass, C., and Selkoe, D.J. 2007. Soluble protein oligomers in neurodegeneration: lessons from the Alzheimer's amyloid β-peptide. *Nat. Rev. Mol. Cell Biol.* **8**:101–112.
13. Zlokovic, B.V., Yamada, Y., Holtzman, D.M., Ghiso, J., and Frangione, B. 2000. Clearance of amyloid β-peptide from brain: transport or metabolism? *Nat. Med.* **6**:718–719.
14. Tanzi, R.E., Moir, R.D., and Wagner, S.L. 2004. Clearance of Alzheimer's Aβ peptide: the many roads to perdition. *Neuron.* **43**:605–608.
15. Zlokovic, B.V. 2008. New therapeutic targets in the neurovascular pathway in Alzheimer's disease. *Neurotherapeutics.* **5**:409–414.
16. Shibata, M., et al. 2000. Clearance of Alzheimer's amyloid β(1-40)-peptide from brain by LDL receptor-related protein-1 at the blood-brain barrier. *J. Clin. Invest.* **106**:1489–1499.
17. Deane, R., et al. 2004. LRP/amyloid beta-peptide interaction mediates differential brain efflux of Abeta isoforms. *Neuron.* **43**:333–344.
18. Cirrito, J.R., et al. 2005. P-glycoprotein deficiency at the blood-brain barrier increases amyloid-beta deposition in an Alzheimer disease mouse model. *J. Clin. Invest.* **115**:3285–3290.
19. Bell, R.D., et al. 2007. Transport pathways for clearance of human Alzheimer's amyloid β-peptide and apolipoproteins E and J in the mouse central nervous system. *J. Cereb. Blood Flow Metab.* **27**:909–918.
20. Nazer, B., Hong, S., and Selkoe, D.J. 2008. LRP promotes endocytosis and degradation, but not transcytosis, of the amyloid-beta peptide in a blood-brain barrier in vitro model. *Neurobiol. Dis.* **30**:94–102.
21. Holtzman, D.M. 2004. In vivo effects of ApoE and clusterin on amyloid-beta metabolism and neuropathology. *J. Mol. Neurosci.* **23**:247–254.
22. Holtzman, D.M., et al. 2000. Apolipoprotein E isoform-dependent amyloid deposition and neuritic degeneration in a mouse model of Alzheimer's disease. *Proc. Natl. Acad. Sci. U. S. A.* **97**:2892–2897.
23. DeMattos, R.B., et al. 2004. ApoE and clusterin cooperatively suppress Aβ levels and deposition: Evidence that apoE regulates extracellular Aβ metabolism in vivo. *Neuron.* **41**:193–202.
24. Zlokovic, B.V. 2005. Neurovascular mechanisms of Alzheimer's neurodegeneration *Trends Neurosci.* **28**:202–208.
25. Jiang, Q., et al. 2008. ApoE promotes the proteolytic degradation of Aβ. *Neuron.* **58**:681–693.
26. Bales, K.R., et al. 1997. Lack of apolipoprotein E dramatically reduces amyloid β-peptide deposition. *Nat. Genet.* **17**:263–264.
27. Holtzman, D.M., et al. 1999. Expression of human apolipoprotein E reduces amyloid-β deposition in a mouse model of Alzheimer's disease. *J. Clin. Invest.* **103**:R15–R21.
28. Fagan, A.M., et al. 2002. Human and murine apoE markedly alters Aβ metabolism before and after plaque formation in a mouse model of Alzheimer's disease. *Neurobiol. Dis.* **9**:305–318.
29. Fryer, J.D., et al. 2003. Apolipoprotein E markedly facilitates age-dependent cerebral amyloid angiopathy and spontaneous hemorrhage in amyloid precursor protein transgenic mice. *J. Neurosci.* **23**:7889–7896.
30. Fryer, J.D., et al. 2005. Human apolipoprotein E4 alters the amyloid-β 40:42 ratio and promotes the formation of cerebral amyloid angiopathy in an amyloid precursor protein transgenic model. *J. Neurosci.* **25**:2803–2810.
31. Xu, F., et al. 2008. Human apolipoprotein E redistributes fibrillar amyloid deposition in Tg-SwDI mice. *J. Neurosci.* **28**:5312–5320.
32. Li, Y., Lu, W., Marzolo, M.P., and Bu, G. 2001. Differential functions of members of the low density lipoprotein receptor family suggested by their distinct endocytosis rates. *J. Biol. Chem.* **276**:18000–18006.
33. Morikawa, M., et al. 2005. Production and characterization of astrocyte-derived human apolipoprotein E isoforms from immortalized astrocytes and their interactions with amyloid-β. *Neurobiol. Dis.* **19**:66–76.
34. Deane, R., et al. 2005. IgG-assisted age-dependent clearance of Alzheimer's amyloid beta peptide by the blood-brain barrier neonatal Fc receptor. *J. Neurosci.* **25**:11495–11503.
35. May, P., Herz, J., and Bock, H.H. 2005. Molecular mechanisms of lipoprotein receptor signalling. *Cell. Mol. Life Sci.* **62**:2325–2338.
36. Zlokovic, B.V., Deane, R., Sallstrom, J., Chow, N., and Miano, J.M. 2005. Neurovascular pathways and Alzheimer amyloid β-peptide. *Brain Pathol.* **15**:78–83.
37. Martel, C.L., et al. 1997. Isoform-specific effects of apolipoproteins E2, E3 and E4 on cerebral capillary sequestration and blood-brain barrier transport of circulating Alzheimer's amyloid beta. *J. Neurochem.* **69**:1995–2004.
38. Roses, A.D. 1996. Apolipoprotein E alleles as risk factors in Alzheimer's disease. *Annu. Rev. Med.* **47**:387–400.
39. Bertram, L., and Tanzi, R.E. 2005. The genetic epidemiology of neurodegenerative disease. *J. Clin. Invest.* **115**:1449–1457.
40. Herz, J., and Hui, D.Y. 2004. Lipoprotein receptors in the vascular wall. *Curr. Opin. Lipidol.* **15**:175–181.
41. Zlokovic, B.V., et al. 1996. Glycoprotein 330/megalin: probable role in receptor-mediated transport of apolipoprotein J alone and in a complex with Alzheimer's disease amyloid beta at the blood-brain and blood-cerebrospinal fluid barriers. *Proc. Natl. Acad. Sci. U. S. A.* **93**:4229–4234.
42. Dehouck, B., et al. 1997. A new function for the LDL receptor: Transcytosis of LDL across the blood-brain barrier. *J. Cell Biol.* **138**:877–889.
43. Kreuter, J. 2001. Nanoparticulate systems for brain delivery of drugs. *Adv. Drug Deliv. Rev.* **47**:65–81.

44. Linton, M.F., et al. 1991. Phenotypes of apolipoprotein B and apolipoprotein E after liver transplantation. *J. Clin. Invest.* **88**:270–281.
45. Wahrle, S.E., and Holtzman, D.M. 2003. Differential metabolism of ApoE isoforms in plasma and CSF. *Exp. Neurol.* **183**:4–6.
46. Ruiz, J., et al. 2005. The apoE isoform binding properties of the VLDL receptor reveal marked differences from LRP and LDL receptor. *J. Lipid Res.* **46**:1721–1731.
47. Mahley, R.W., and Huang, Y. 1999. Apolipoprotein E: from atherosclerosis to Alzheimer's disease and beyond. *Curr. Opin. Lipidol.* **10**:207–217.
48. Fryer, J.D., et al. 2005. The low density lipoprotein receptor regulates the level of central nervous system human and murine apolipoprotein E but does not modify amyloid plaque pathology in PDAPP mice. *J. Biol. Chem.* **280**:25754–25759.
49. Kowal, R.C., et al. 1990. Opposing effects of apolipoproteins E and C on lipoprotein binding to low density lipoprotein receptor-related protein. *J. Biol. Chem.* **265**:10771–10779.
50. Narita, M., et al. 2002. Cellular catabolism of lipid poor apolipoprotein E via cell surface LDL receptor-related protein. *J. Biochem.* **132**:743–749.
51. Sagare, A., et al. 2007. Clearance of amyloid-β by circulating lipoprotein receptors. *Nat. Med.* **13**:1029–1031.
52. Strittmatter, W.J., et al. 1993. Apolipoprotein E: High-avidity binding to β-amyloid and increased frequency of type 4 allele in late-onset familial Alzheimer's disease. *Proc. Natl. Acad. Sci. U. S. A.* **90**:1977–1981.
53. LaDu, M.J., et al. 1995. Purification of apolipoprotein E attenuates isoform-specific binding to beta-amyloid. *J. Biol. Chem.* **270**:9039–9042.
54. Tokuda, T., et al. 2000. Lipidation of apolipoprotein E influences its isoform-specific interaction with Alzheimer's amyloid beta peptides. *Biochem. J.* **348**:359–365.
55. Wyss-Coray, T., et al. 2003. Adult mouse astrocyte degrade amyloid-β in vitro and in situ. *Nat. Med.* **9**:453–457.
56. Koistinaho, M., et al. 2004. Apolipoprotein E promotes astrocyte colocalization and degradation of deposited amyloid-β peptides. *Nat. Med.* **10**:719–726.
57. Cole, G.M., and Ard, M.D. 2000. Influence of lipoproteins on microglial degradation of Alzheimer's amyloid beta protein. *Microsc. Res. Tech.* **50**:316–324.
58. Cirrito, J.R., et al. 2003. In vivo assessment of brain interstitial fluid with microdialysis reveals plaque-associated changes in amyloid-β metabolism and half-life. *J. Neurosci.* **23**:8844–8853.
59. Wilhelmus, M.M.M., et al. 2005. Apolipoprotein E genotype regulates amyloid-β cytotoxicity. *J. Neurosci.* **25**:3621–3627.
60. Hatters, D.M., Zhong, N., Rutenber, E., and Weisgraber, K.H. 2006. Amino-terminal domain stability mediates apolipoprotein E aggregation into neurotoxic fibrils. *J. Mol. Biol.* **361**:932–944.
61. Ye, S., et al. 2005. Apolipoprotein (apo) E4 enhances amyloid β peptide production in cultured neuronal cells: ApoE structure as a potential therapeutic target. *Proc. Natl. Acad. Sci. U. S. A.* **102**:18700–18705.
62. Sadowski, M.J., et al. 2006. Blocking the apolipoprotein E/amyloid-β interaction as potential therapeutic approach for Alzheimer's disease. *Proc. Natl. Acad. Sci. U. S. A.* **103**:18787–18792.
63. Mahley, R.W., Weisgraber, K.H., and Huang, Y. 2006. Apolipoprotein E4: A causative factor and therapeutic target in neuropathology, including Alzheimer's disease. *Proc. Natl. Acad. Sci. U. S. A.* **103**:5644–5651.
64. Cedazo-Mínguez, A. 2007. Apolipoprotein E and Alzheimer's disease: molecular mechanisms and therapeutic opportunities. *J. Cell. Mol. Med.* **11**:1227–1238.
65. Thorell, J.I., and Johansson, B.G. 1971. Enzymatic iodination of polypeptides with ^{125}I to high specific activity. *Biochim. Biophys. Acta.* **251**:363–366.
66. LaRue, B., et al. 2004. Method for measurement of the blood-brain barrier permeability in the perfused mouse brain: application to amyloid-β peptide in wild type and Alzheimer's Tg2576 mice. *J. Neurosci. Methods.* **138**:233–242.
67. Wu, Z., Hofman, F.M., and Zlokovic, B.V. 2003. A simple method for isolation and characterization of mouse brain microvascular endothelial cells. *J. Neurosci. Methods.* **130**:53–63.